Discovery of Fe-Ce oxide / $BiVO_4$ photoanodes through combinatorial exploration of Ni-Fe-Co-Ce oxide coatings

Aniketa Shinde[‡,†], *Dan Guevarra*[‡,†], *Guiji Liu*[‖], *Ian D. Sharp*[‖], *Francesca M. Toma*[‖,*], *John M. Gregoire*[‡,*], *Joel A. Haber*[‡,*]

[‡]Joint Center for Artificial Photosynthesis, California Institute of Technology; Pasadena, CA 91125, USA

[‖]Joint Center for Artificial Photosynthesis & Chemical Sciences Division, Lawrence Berkeley National Laboratory, Berkeley, CA 94720, USA

Corresponding authors:
* E-mail: fmtoma@lbl.gov
* E-mail: gregoire@caltech.edu
* E-mail: jahaber@caltech.edu

EXPERIMENTAL DETAILS

$BiVO_4$ and (Ni-Fe-Co-Ce)O_x Library Synthesis

The fluorine doped tin oxide (FTO)-coated side of a 10 cm × 10 cm glass plate (TEC-15 Sigma Aldrich) was coated with $BiVO_4$ following a literature protocol,[23] after washing with isopropanol (Sigma Aldrich, ≥98%), detergent (Alconex) in deionized water, and pure deionized water, drying with a nitrogen gun, and 10 min of treatment with an ozone cleaner (Jelight Model 42). The deposition solution was prepared from 15 mL of a 0.2 M solution of bismuth (III) nitrate pentahydrate (Sigma Aldrich, ≥98%) in acetylacetone (Sigma Aldrich, ≥99%) and 100 mL of a 0.03 M solution of vanadium (IV)-oxy acetylacetonate in acetylacetone which were prepared separately and sonicated for 10 min. Then, the two solutions were mixed together and sonicated for an additional 5 min. Enough of the resulting solution to homogeneously cover the whole surface (1-1.2 mL) was filtered with 0.45 µm nylon filters (Thermo Fisher Scientific), and dispensed onto the 10 cm × 10 cm FTO/glass plate. The substrate was then spun two times at 1000 rpm for 6 s on a spin coater (Laurell Technologies) with an acceleration rate of 150 rpm/s, then annealed in air for 10 min at 500 °C in a muffle furnace (Cole-Parmer). This spin-coating then annealing procedure was repeated nine times. After the last spin-coating cycle, the substrate was annealed for 2 h at 500 °C to yield a final thickness of ~50 nm. Thickness determination was performed by Rutherford Backscattering Spectrometry (RBS), where He^+ ions were accelerated to 3040 keV on a 5SDH pelletron tandem accelerator manufactured by National Electrostatics Corporation (NEC) with a sample tilt of 30-60° and backscattered ion detection at 165° using a Si surface barrier detector. Data fitting was performed with SIMNRA software. Production of phase-pure monoclinic $BiVO_4$ was verified by X-ray Diffraction (XRD) analysis using a Rigaku SmartLab diffractometer configured with parallel beam optics (see Figure S1).

The array of metal oxide coatings was deposited onto the light absorber plate to create a library of photoanode assemblies. A library of electrocatalysts was prepared by depositing a duplicate array of metal oxides onto an FTO-coated glass plate (without $BiVO_4$). The composition library of mixed-metal oxide catalysts containing Ni, Fe, Co, and Ce was synthesized as a discrete library with 10 atom % composition steps in each element. Each of the 286 compositions in this pseudo-quaternary composition space was deposited at 3 different catalyst loadings (designated L1, L2, and L3). The array of 858 metal oxide samples was deposited by inkjet printing at a resolution of 2880 × 1440 dpi, as described previously.[41,44] Precursor inks containing a single metal were prepared by mixing 5 mmol of each metal precursor with 0.80 g Pluronic F127 (Aldrich), 1.0 mL glacial acetic acid (T.J. Baker, Inc.), 0.40 mL of concentrated HNO_3 (EMD), and 30 mL of 200 proof ethanol (Koptec). The metal precursors were $Ni(NO_3)_2$-$6H_2O$ (1.59 g, ≥98.5%, Sigma Aldrich), $Fe(NO_3)_3$-$9H_2O$ (2.13 g, ≥98%, Sigma Aldrich), $Co(NO_3)_2$-$6H_2O$ (1.49 g, 99.999%, Sigma Aldrich), and $Ce(NO_3)_3$-$6H_2O$ (2.22 g, >99.0%, Sigma Aldrich). After the composition-loading library was inkjet-printed, the inks were dried and the metal precursors converted to metal oxides by calcination in air at 40 °C for 20 h, then at 70 °C for 27 h, followed by a 5 h ramp and 5 h soak at 350 °C.

High Throughput Photoelectrochemistry

The PEC and spectroscopic properties of the photoanode library were characterized using a custom-built SDC combined with optical illumination and detection, as described previously.[46] A Ag/AgCl reference electrode and Pt counter electrode form a 3-electrode cell that is controlled by a Gamry G 300 potentiostat and custom software. Electrochemical experiments were performed in aqueous pH 13 electrolyte (0.1 M sodium hydroxide with 0.5 M sodium sulfate as a supporting electrolyte).

The SDC included a 0.4 mm-diameter optical fiber that was integrated into the central port of the SDC and coupled to a xenon arc lamp (Newport 66921, 450W) that was coupled with a liquid water filter to remove infra-red radiation (Oriel Instruments, 6123NS), neutral density filter (Rolyn Optics, #66.0220 50%T), and AM 1.5 filter (Newport, 81094). The fiber was placed approximately 1 mm above the library plate, resulting in an illumination footprint diameter of approximately 1 mm. The lamp was calibrated according to the protocol described in the supplementary information provided with reference 7. The resulting illumination irradiance was approximately 3.2 times that of AM 1.5 over the visible and ultraviolet wavelengths (390-900 nm) and nearly 4 times greater than that of ASTM 6173-03 Global AM 1.5 over the wavelength range absorbed by $BiVO_4$, (390-600 nm).

The PEC properties of the photoanode library were measured by toggled-illumination CVs. The potential was swept from 1.23 to 0.585 V and back to 1.23 V vs. RHE (0 to -0.645 V and back to 0 V vs. O_2/H_2O) at a scan rate of 0.02 V s^{-1}, while illumination was toggled at 0.5 Hz (1.34 s on, 0.67 s off). Data processing for the toggled-illumination CVs is described in the supplementary information provided with reference 7. Due to significant transients in the illuminated current during the cathodic sweep, all PEC properties of the photoanode library are obtained from the anodic sweep. Photocurrent density ($J_{photo}(V)$) is the difference between the illuminated and dark current density signals.

$J_{photo}(V)$ was used to determine J_{O_2/H_2O}, E_{OC}, and P_{max}. Using J_{photo} at 1.23 V vs. RHE (0 V vs. O_2/H_2O), the photo-generated current density at the Nernstian potential for water oxidation, J_{O_2/H_2O} was calculated. The photocurrent remained positive during the entire CV for many photoanodes, resulting in an approximation of the open circuit photovoltage (E_{OC}) that required extrapolation of the photocurrent signal, also discussed in the SI. J_{photo} was analyzed to calculate the maximum power point for each photoanode with respect to OER photoelectrocatalysis, which refers to specific values of E (E_{mp}) and J_{photo} (J_{mp}) that correspond to the maximum PEC power generation (P_{max}), assuming 100% Faradaic yield for the OER.

The catalyst library was characterized with the same experimental setup to perform illuminated CA measurements held at an OER overpotential (η_{OER}) of 0.35 V for 25 s. Catalytic current density (J_{cat}) was the average current density over the last 1 s of the measurement.

In situ optical measurements

During each CA measurement on the catalyst library, the transmitted light was collected by an integrating sphere (Spectral Products AT-IS-1) placed 1 mm below the library plate

and fiber-coupled to a UV-vis spectrometer (Spectral Products SM303). SDC measurements were performed in an enclosure to block ambient light. Transmission spectra were averaged over the last 2 s at the end of the CA measurement to provide the fractional transmission spectrum (T_{cat}) of each catalyst at 1.58 V vs. RHE (0.35 V vs. O_2/H_2O). Reference transmission spectra were collected from bare regions of FTO-coated glass on the catalyst library plate and combined with the dark signal from the spectrometer to determine the fractional transmission ($T(\lambda)$) for each spectral measurement, as detailed in the supplementary information provided with reference 7

High-throughput screen of photostability

Toggled illumination CA measurements at an applied potential close to the maximum power point were utilized for high throughput evaluation of the stability of the catalyst on $BiVO_4$ photoanodes. Utilizing the pulsed illumination CV data collected on the L2 samples, the top performing samples were evaluated to determine P_{max} and the corresponding E_{mp}. The E_{mp} values for the samples in the 99th percentile of P_{max} range from -0.35 to -0.43 V vs O_2/H_2O with a mean value of -0.39 V vs O_2/H_2O. The photoanode samples selected for the toggled illumination CA measurements were those yielding $J_{photo} \geq 0.19$ mA cm^{-2} at 0.43 V vs O_2/H_2O, the highest E_{mp} value exhibited in the 99th percentile of P_{max}.

Using this down-selection criteria, toggled illumination CA measurements were collected on 159 (56%) of the 286 fresh samples in the duplicate L2 library. The CAs were measured at 0.80 V vs RHE (-0.43 V vs OER) using 1.34 s light on and 0.67 s light off toggling. After an initial 29.5 s CA, a requirement that $J_{photo} \geq 0.38$ mA cm^{-2} was applied as an on-the-fly down selection criteria. The second CA was continued on 86 samples passing this criterion for an additional 150 s, for a total stability measurement of 180 seconds.

Optical transmission efficiency

We define an optical parameter useful for evaluating the performance of catalysts based on optical transmission which determines the effective wavelengths available for absorption by the underlying $BiVO_4$. For the photoanode library, the number of photons expected to be absorbed by the $BiVO_4$ can be calculated from the product of the fractional transmission spectrum of a catalyst (T_{cat}), the fractional absorption of the $BiVO_4$ ($\boldsymbol{A}_{\mathrm{BVO}}(\lambda)$), and the photon flux of the incident light ($\boldsymbol{N}_{\mathrm{Lamp}}(\lambda)$). The corresponding optical transmission efficiency ($\alpha_{T,cat}$, Eq 4) of the catalyst is given by the fractional transmission of photons that are expected to be absorbed by the $BiVO_4$:

$$\alpha_{T,cat} = \int_{\lambda_1}^{\lambda_2} T_{cat}(\lambda)\, \boldsymbol{A}_{\mathrm{BVO}}(\lambda)\, \boldsymbol{N}_{\mathrm{Lamp}}(\lambda)\, \mathrm{d}\lambda \,/\, \int_{\lambda_1}^{\lambda_2} \boldsymbol{A}_{\mathrm{BVO}}(\lambda)\, \boldsymbol{N}_{\mathrm{Lamp}}(\lambda)\, \mathrm{d}\lambda. \qquad [4]$$

The wavelength integration range of 390 nm to 600 nm was chosen as the range absorbable by $BiVO_4$.

Scale-up and traditional photoelectrochemistry

Identical $BiVO_4$ film preparation, inkjet printing, and thermal processing conditions were used to prepare approximately 1 cm^2 photoanodes. The $Fe_{0.5}Ce_{0.5}O_x$ catalyst was also deposited through PED in an undivided cell containing 0.05 M iron(III)nitrate nonahydrate (Sigma Aldrich, ≥98%) and 0.05 M cerium(III)nitrate hexahydrate (Alfa Aesar, 99.998%), using a Ag/AgCl reference electrode, a Pt mesh counter electrode, and $BiVO_4$ coated FTO/glass as the working electrode. The electrodes were back-side illuminated with simulated AM 1.5G 1 Sun solar irradiation while a potential of 1.3 V vs. Ag/AgCl was applied for 5 min.

An approximately 0.3 cm wide strip of the $BiVO_4$ thin film was removed by chemical etching using 0.1 M HCl (Sigma Aldrich, ACS reagent, 37%) to expose FTO. A Cu wire was connected to the exposed FTO using silver conductive epoxy (Circuit Works, CW2400), and the electrode with the attached wire was dried for 20 min at 60 °C. The wire was isolated with a glass tube, and the Cu wire, silver epoxy, and exposed FTO were all sealed together with the glass tube using Loctite 615 Hysol epoxy. Optical scanning of the assembled photoelectrodes and digital image analysis with standard software (Image J) was used to determine the exposed surface areas. All PEC measurements were performed in a three electrode PEC cell with a planar quartz window (5 cm^2) using a BioLogic SP200 potentiostat. In the three-electrode PEC cell, the $BiVO_4$-catalyst photoanode, a coiled Pt wire, and a Ag/AgCl (3 M NaCl, BASI) were the working, counter, and reference electrodes, respectively. Measurements were performed in 0.1 M NaOH (Sigma Aldrich, ACS reagent, ≥97%) with and without the addition of 0.1 M Na_2SO_3 (Sigma Aldrich, ACS reagent, ≥98%) as sacrificial reagent. Simulated AM 1.5 light (Solar Light) adjusted to 100 mW/cm^2 using a calibrated Si PV cell (SolarSim calibration, Newport) was used for all measurements under illumination.

CV measurements were collected from the open circuit potential to 1.7 V vs. RHE (0.47 V vs. O_2/H_2O) at a scan rate of 100 mV s^{-1} to establish photoelectrochemical performance. Dark CV measurements were performed immediately before the illuminated CV measurements for both catalyst-coated and bare $BiVO_4$ electrodes. After the CV experiments, the photoelectrochemical stability of these electrodes was evaluated with a CA measurement at an applied bias of 1.23 V vs. RHE (0 V vs. O_2/H_2O) in the pH 13, 0.1 M NaOH electrolyte.

X-ray photoelectron spectroscopy (XPS)

X-ray photoelectron spectroscopy (XPS) was performed using a 300 micrometer diameter monochromatized Al Kα source (hν = 1486.6 eV), operated at 225 W, on a Kratos Axis Ultra DLD system at a takeoff angle of 0º relative to the surface normal, and pass energy for narrow scan spectra of 20 eV, corresponding to an instrument resolution of approximately 600 meV. Spectral fitting was done using Casa XPS analysis software. Spectral positions were corrected using adventitious carbon by shifting the C 1s core level position to 284.8 eV and curves were fit with quasi-Voigt lines following Shirley background subtraction. The chemical quantification (expressed in atomic %) was performed normalizing the photoelectron peaks' areas by their corresponding sensitivity factors.

Table S2 summarizes this composition analysis for both IJP and PED samples where XPS spectra were acquired at 3 different locations on each electrode, and it is important to note that the locations for post-PEC characterization may be different from the pre-PEC positions. The compositions were calculated assuming separate phases of (Fe-Ce)O_x and $BiVO_4$. Due to variations in each coating thickness and the bilayer structure of the photoanodes, additional characterization and sophisticated modelling would be required to perform detailed compositional analyses. The uncertainties noted in the table reflect the standard deviations of each set of 3 composition measurements. Systematic errors due to insufficient structure and chemistry models are expected to be approximately 10 atomic % and may change between pre-PEC and post-PEC measurements due to $BiVO_4$ corrosion (as shown in Fig. S8 for the IJP coating) and other morphology changes. Table S2 suggests that the Fe concentration increases slightly during PEC experiments for the IJ coating but decreases slightly for PED coatings, bringing into question whether these different composition quantifications are due to the substantially different morphologies of the coatings. The most substantial and consistent result from the XPS characterization is the loss of V from the near surface region during PEC experiments, which leads to an increase in the Bi concentration and is consistent with both the XRF results of Fig. S8 and recent studies of (photo)corrosion of $BiVO_4$.

MATERIAL CHARACTERIZATION

This section provides supplementary information on quality control and visualization of the composition space. Table S1 lists the definition of composition symbols used to map the 4-component composition space as a series of 12 pseudo-ternary composition triangles. Figure S1 shows the results of XRF mapping of the Bi concentration in the $BiVO_4$ film prior to deposition of the catalyst library. The combinatorial photoelectrochemical measurements rely on a uniform light absorber layer under the entire library, which is demonstrated in this measurement.

Table S1. Definition of composition labels in Fig. 4a, where M' is the most M-rich composition with at least 0.1 of each element and M'' is the most M-rich composition with at least 0.2 of each element. The entire quaternary composition space with 0.1 composition intervals can be considered as the combined set of all pseudo-ternary combinations of (Fe-Ce-Ni-Co)O_x, of Fe′-Ce′-Ni′-Co′, and of Fe″-Ce″-Ni″-Co″.

Fe′	$Fe_{0.7}Ce_{0.1}Ni_{0.1}Co_{0.1}O_x$
Ce′	$Ce_{0.7}Fe_{0.1}Ni_{0.1}Co_{0.1}O_x$
Ni'	$Ni_{0.7}Ce_{0.1}Fe_{0.1}Co_{0.1}O_x$
Co′	$Co_{0.7}Ce_{0.1}Ni_{0.1}Fe_{0.1}O_x$
Fe″	$Fe_{0.4}Ce_{0.2}Ni_{0.2}Co_{0.2}O_x$
Ce″	$Ce_{0.4}Fe_{0.2}Ni_{0.2}Co_{0.2}O_x$
Ni″	$Ni_{0.4}Ce_{0.2}Fe_{0.2}Co_{0.2}O_x$
Co″	$Co_{0.4}Ce_{0.2}Ni_{0.2}Fe_{0.2}O_x$

Table S2. Integrated raw peak areas and calculated atomic percentages for Fe, Ce, Bi, and V for different coatings on $BiVO_4$ pre- and post-PEC stability testing. The uncertainties were calcualted as the standard deviations from triplicate measurements and do not reflect substantial systematic uncertanties in composition quantification.

		Atomic % ($FeCeO_x$ and $BiVO_4$ calculated separately)			
		Fe (2p)	**Ce (3d)**	**Bi (4f)**	**V (2p)**
IJP $Fe_{0.5}Ce_{0.5}O_x$-L1	Pre-PEC	36.5 ± 0.6%	63.5 ± 0.6%	56 ± 3%	44 ± 3%
	Post-PEC	42.5 ± 0.8%	57.1 ± 0.8%	85 ± 2%	14 ± 2%
PED $Fe_{0.5}Ce_{0.5}O_x$-A	Pre-PEC	49 ± 3 %	51 ± 3%	59.8 ±0.2%	40.2 ± 0.2%
	Post-PEC	31 ± 6%	69 ± 6%	75.6 ± 0.3%	24.3 ± 0.3%
PED $Fe_{0.5}Ce_{0.5}O_x$-B	Pre-PEC	42 ± 2%	58 ± 3%	59.2 ± 0.3%	40.8 ± 0.3%
	Post-PEC	37 ±2 %	63 ± 2%	75.7 ± 0.1%	24.3 ± 0.1%

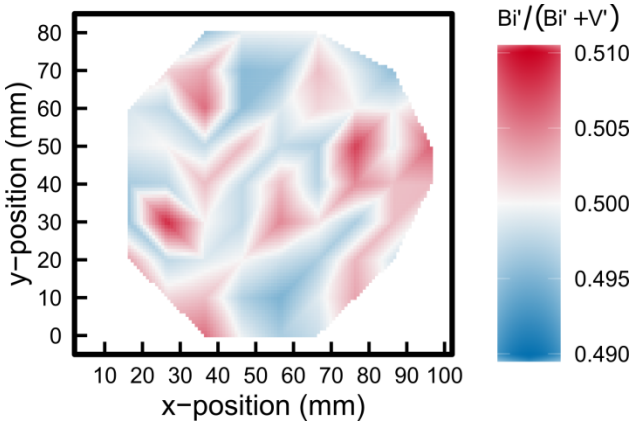

Figure S1. XRF mapping of the Bi:(Bi+V) composition in the spin-coated $BiVO_4$ film prior to deposition of the metal oxide library. The small deviations from 0.5 are within the noise of the measurement, and the lack of a spatial gradient in composition demonstrates the uniformity of the spin coating process.

Optical data processing

The calibration of the illumination source used in the high throughput experiments, definition of the lamp spectra used in the calculations of optical properties, and representative spectra to illustrate the data processing have previously been reported in detail.[13] No changes were made for the measurements reported here.

Electrochemical data processing

The automated data processing of the toggled illumination cyclic voltammetry (CV) measurements used to extract the photocurrent density, $J_{photo}(V)$, which is further analyzed to extract $P_{max}, J_{O_2/H_2O}$, J_{mp}, and V_{mp}, has previously been described in detail.[13] The resulting figures of merit as a function of composition and loading for the Ni-Fe-Co-Ce oxide libraries is presented below.

Photoanode figures of merit for all catalyst loadings L1, L2, L3

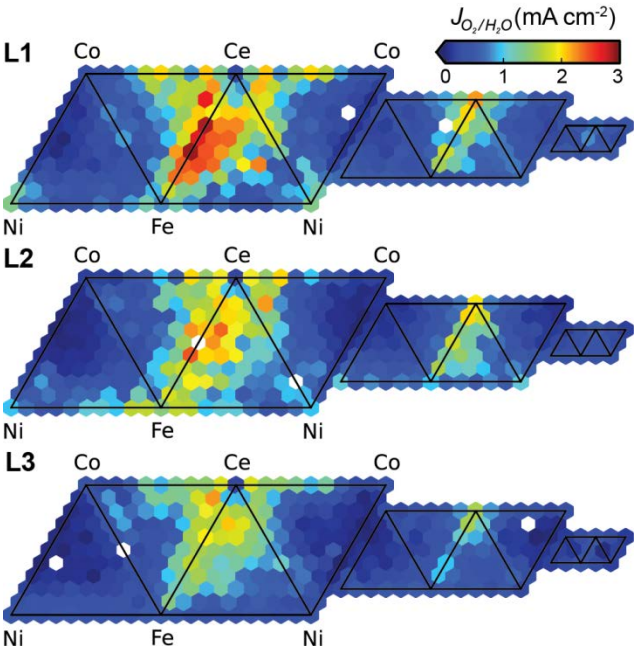

Figure S2. J_{O_2/H_2O} for all three loadings of the (Ni-Fe-Co-Ce)O_x photoanode library.

Electrocatalyst figures of merit for all catalyst loadings L1, L2, L3

The metal oxide library was synthesized on an FTO-coated glass plate to characterize OER electrocatalytic performance and optical transparency under operating conditions. The maps for loading L1 are shown in the manuscript (Fig. 7) and the full library maps for the catalytic current density and transmission efficiency of $BiVO_4$-absorbable photons are shown in Figures S3 and S4, respectively.

In Figure S5, the combined catalyst efficiency is mapped over its 2 constituent catalyst performance metrics from Figures S3 and S4. The combined catalyst efficiency is mapped over thickness and composition space in Figure S6. The metric for quantifying photoanode performance enhancement with respect to the combined catalyst efficiency is mapped in Figure S7. We note that for Figures S3, S4, S6, and S7, the data for loading L1 is identical to that of the manuscript figures.

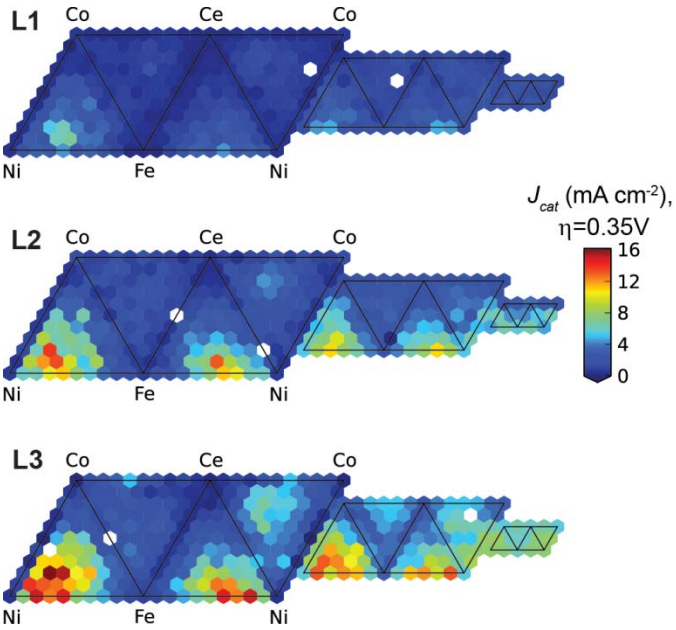

Figure S3. Catalytic current density J at η_{OER} = 0.35 V overpotential for all three loadings in the electrocatalyst library.

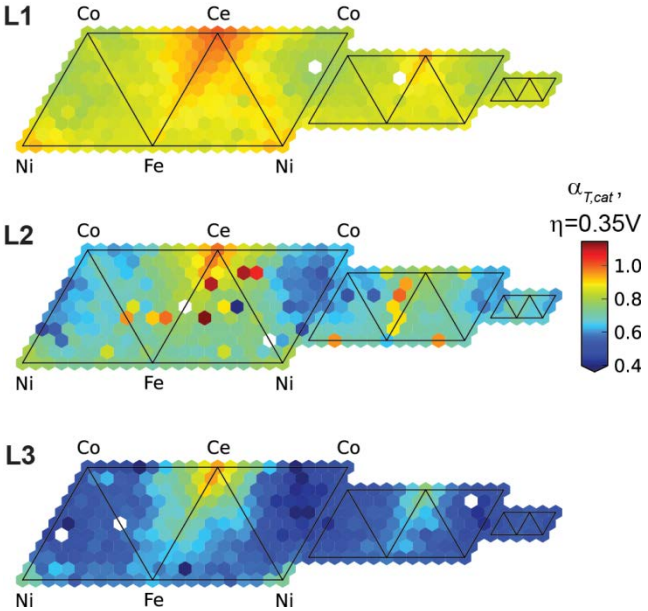

Figure S4. Optical transmission efficiency $\alpha_{T,cat}$ of the catalyst library at all three loadings.

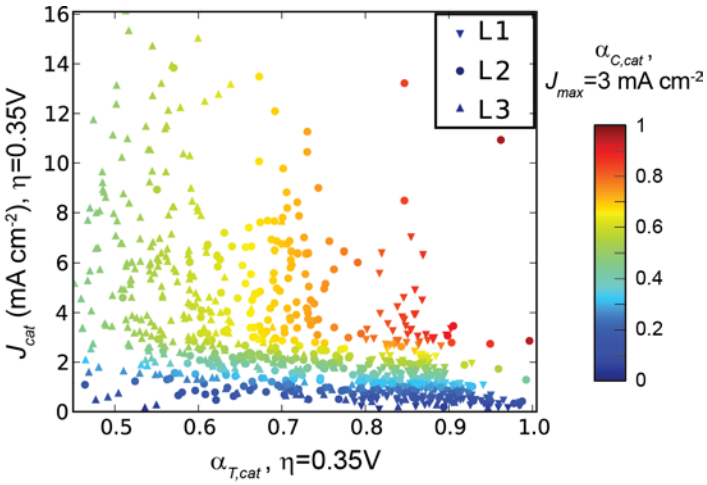

Figure S5. Scatter plot of the unitless combined catalyst efficiency $\alpha_{\mathrm{C,cat}}$ of all three catalyst loadings. Vertical axis is current density J at η_{OER} = 0.35 V from Figure S3 and horizontal axis is optical transmission efficiency $\alpha_{T,cat}$ from Figure S4.

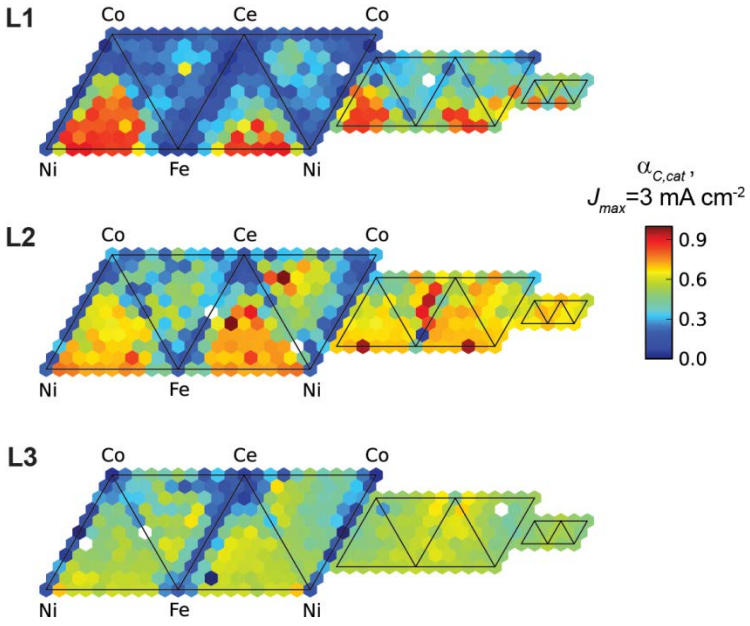

Figure S6. Combined catalyst efficiency $\alpha_{C,cat}$ of the catalyst library at all three loadings for J_{max} = 3.8 mA cm^{-2}.

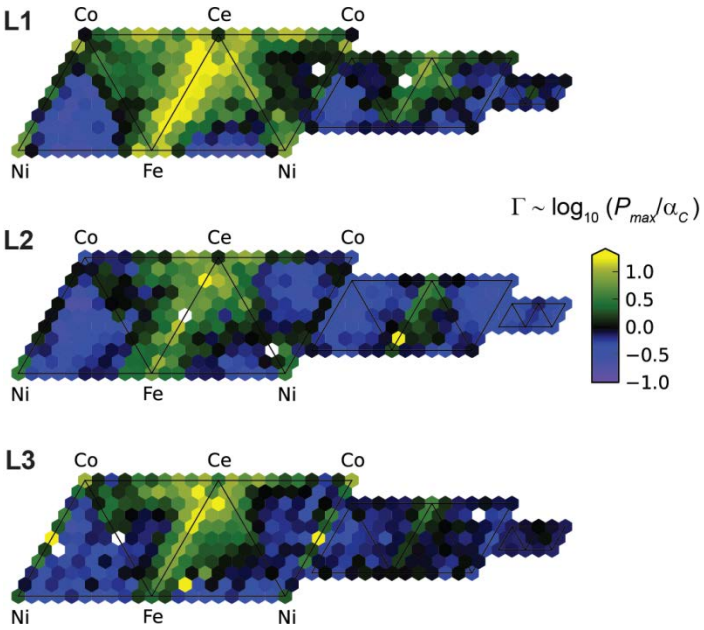

Figure S7. Γ for all three loadings where $\Gamma = \Gamma' - \text{median}(\Gamma')$ and $\Gamma' = \log_{10}\left(\alpha_{C,cat}/P_{\max}\right)$, as discussed in the manuscript.

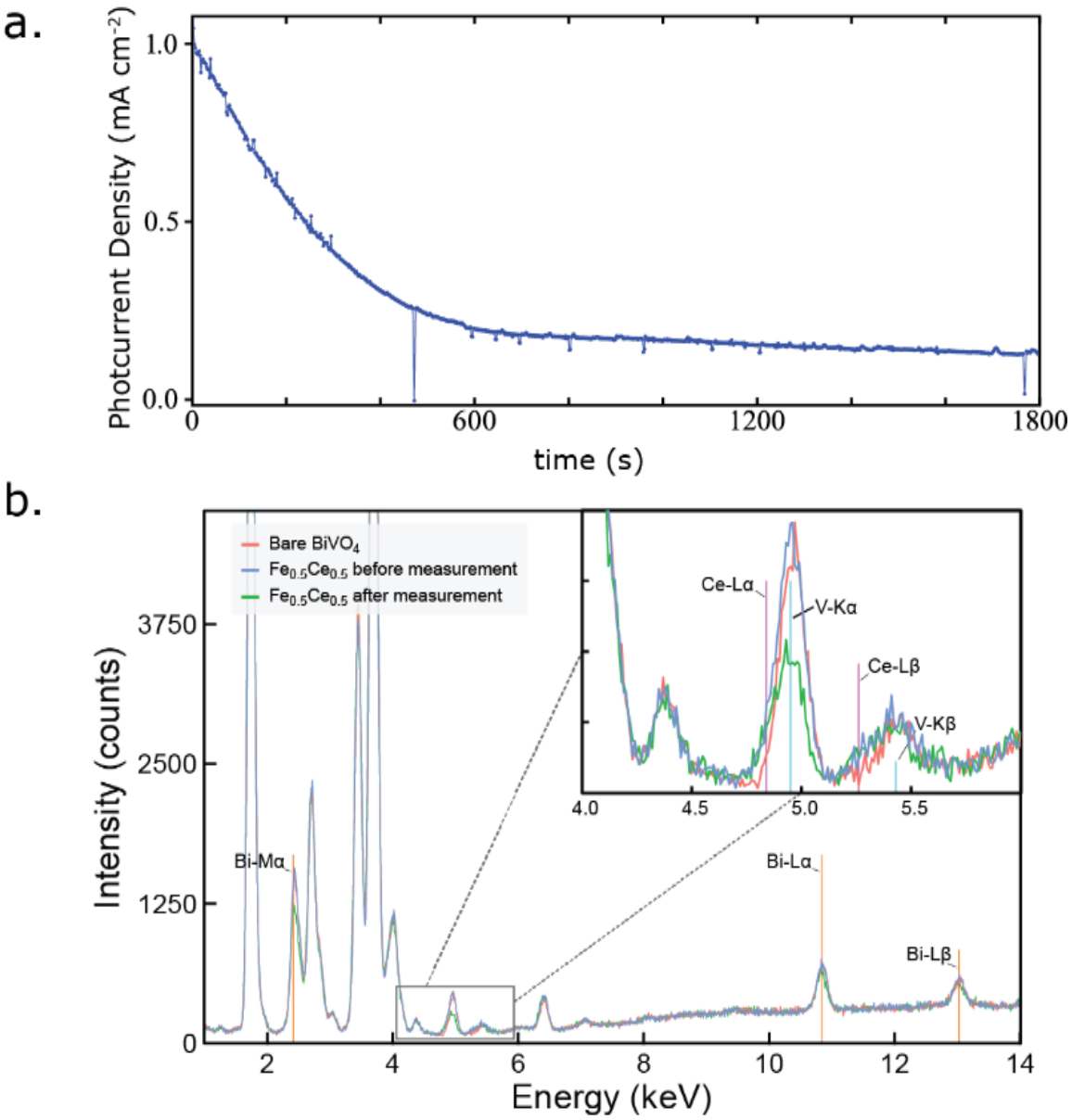

Figure S8. (a) Chopped-illumnation CA result for 30 minute measurement acquired on the $Fe_{0.5}Ce_{0.5}O_x$-L1 sample after the high throughput CV experiment. (b) XRF measurements of the sample before coating deposition (red), after coating deposition (blue), and after CV and CA experiments (green). The strongest XRF peaks are from the subtrate and include Sn, Si, Ca, and a smaller peak from Fe in the glass, which precludes characterization of Fe in the coating. The Bi M, Bi L, and V K peaks were analyzed to quantify elemental loss from the PEC experiments. The primary Ce L peaks overlap with V K peaks, the inset shows the presence of Ce signal after coating deposition and its invariance after PEC experiments.

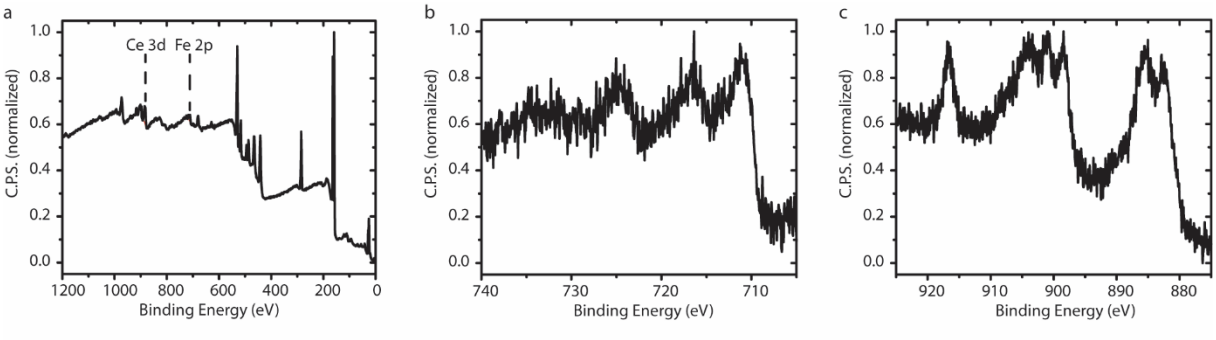

Figure S9. XPS of BiVO4 with PED deposited (Fe-Ce)O_x catalyst. (a) Survey spectrum. (b) High resolution Fe 2p core level. (c) High resolution Ce 3d core level. Analysis of Fe and Ce atomic concentration for a different set of samples gives Fe = 54 ± 7 at% and Ce = 46 ± 7 at%.